with other free SH-bearing molecules in the cell, such as cysteine and SH residues in proteins, yet their relatively low concentrations contribute only little towards changing the reduction potential of the cell upon oxidation. The reduction potential of cells was proposed to reflect their growth cycle. Accordingly, the reduction potential of proliferating cells (pH 7.0) is E_{GSH} −240 mV. Increased values (E_{GSH} −200 mV) represent differentiation, and a further oxidative shift to a higher value (E_{GSH} −170 mV) elicits apoptosis [27]. In this study, we aimed to examine the initial events leading to apoptosis upon allicin treatment and the dependence of the apoptotic pathway on the reduction potential of cells.

2. Materials and methods

Alliin was synthesized from L-cysteine and allyl bromide followed by H_2O_2 oxidation [30]. Allicin (purity ~98%) was produced by applying synthetic alliin onto an immobilized alliinase column and its concentration was determined by high-performance liquid chromatography, as previously described [31].

2,3-Bis (2-methoxy-4-nitro-5-sulfophenyl)-2 *H*-tetrazolium-5-carboxanilide (XTT) sodium salt; D,L-buthionine *S*, *R*-sulfoximine (BSO); cyclosporin A (CsA); *N*-acetyl-L-cysteine (NAC); 5,5′-dithiobis-(2-nitrobenzoic acid) (DTNB); metaphosphoric acid; phenazine methosulfate (PMS) and 2-vinylpyridine were purchased from Sigma Chemical (St. Louis, MO, USA).

2.1. Cell culture, cell viability and morphological studies.

HL60 human promyelocytic leukemia-derived cells and U937 human myelomonocytic cells were maintained in RPMI-1640 supplemented with 2 mM L-glutamine, 10% (v/v) fetal bovine serum and antibiotics. Cell viability was measured using the XTT assay, based on the reduction of tetrazolium salt to soluble formazan compounds by mitochondrial enzymes. Cells (15.000–20.000 cells/well) were seeded in a 96-well plate. After 16-h incubation with allicin, in the presence or absence of NAC (0.1–1.0 mM) or after 16 h incubation with BSO (0.1 mM) alone, 50 μl of XTT/PMS mixture (50 μM PMS, 0.1% XTT in medium) were added onto the cells. After an incubation period of 3–4 h at 37°C, the absorbance of the samples was measured in an enzyme-linked immunosorbent assay (ELISA) reader at 450 nm. SDS (1%, 10 μl/well) was added to reference wells before adding the XTT/PMS solution.

HL60 cells (300,000/ml) were pretreated with CsA for 1 h. Cells were seeded in a 96-well plate (20,000 cells/well) in the presence of allicin. The viability was tested by the XTT assay. The analysis of apoptotic morphological changes was done by staining cells with Hoechst 33342 at 37°C for 30 min in medium, washing with phosphate-buffered saline (PBS) and examining by fluorescence microscopy. For evaluating DNA ladder formation, cellular DNA was extracted from cells by ethanol precipitation of the phenol/chloroform extract [32]. After electrophoresis (5–10 μg DNA/lane) on an agarose (2.5%) gel, DNA was visualized by ethidium bromide staining.

Mitochondrial membrane potential was measured by using the fluorescent dye, Mito Tracker Red CMXRos (Molecular Probes, Eugene, OR, USA) that accumulates selectively in active mitochondria. Cells were washed with medium, incubated with Mito-Tracker Red CMXRos for 30 min at 37°C, washed with PBS and examined under fluorescence microscopy (Olympus, Tokyo).

Mitochondria were prepared from cultured cells (5–10×10^7) as described elsewhere [33]. Cells were harvested and washed with PBS (600 g, 7 min). Cell pellets were suspended in 0.5 ml cold HIM buffer (200 mM mannitol, 70 mM sucrose, 1 mM EGTA, 10 mM HEPES-KOH buffer, pH 7.5) containing protease inhibitors, incubated 30 min on ice and homogenized by multiple passages through a 25-gauge needle (5/8 in.). Nuclei and unbroken cells were removed (1300 g, 8 min at 4°C). Protein and free SH were determined in the cytosol, supernatant (10,000 g, 30 min at 4°C) and in the mitochondria-enriched fraction (pellet, dissolved in HIM buffer containing 1% Triton X-100). Protein assay was done with the Biuret Reagent [34] or the BCA protein assay kit (Pierce, Rockford, IL, USA).

2.2. Cell cycle analysis

HL60 cells were pretreated with CsA (5 μM, 1 h) and then cultured further for 20 h in the presence or absence of allicin. After harvesting, washing and resuspending in 0.25 ml PBS, an equal volume of 0.005% propidium iodide solution containing 0.01% heated-RNase A and 0.3% Triton X-100 was added. Cells were analyzed by flow cytometry using fluorescence-activated cell sorting (Becton Dickinson FACScan Instrument using CellQuest software (BD Bioscience, San Jose, CA, USA).

2.3. Electrophoresis and Western blot analysis

Cell pellet was resuspended in lysis buffers A or B [32]. Lysis buffer A (2×PBS, 0.1% sodium dodecyl sulfate (SDS), 1% Nonidet P-40, 0.5% sodium deoxycholate) containing protease inhibitors was used to analyze of caspases 3, 8 and 9. Lysis buffer B (250 mM sucrose, 20 mM HEPES-KOH buffer, pH 7.5, 10 mM KCl, 1.5 mM $MgCl_2$, 1 mM EDTA, 1 mM EGTA, 1 mM DTT) containing protease inhibitors was used to analyze the presence of cytochrome *c* in the cytosol as described above (Section 2.2), After centrifugation (10,000*g*, 30 min, 4°C) the supernatant was separated by SDS-polyacrylamide gel electrophoresis using 15% gel and transferred electrophoretically onto a PVDF membrane (Du Pont, Boston, MA, USA). The membrane was incubated overnight at 4°C with the following antihuman antibodies: anti β-actin (Sigma–Aldrich), anti-caspase 3 (Santa Cruz Biotechnology, Santa Cruz, CA, USA), anti-caspase 8 (MBL, Nagoya, Japan), anti caspase-9 (Novus Biological,

Littleton, CO, USA) and anti cytochrome *c* (Upstate Biotechnology, Lake Placid, NY, USA). The membranes were washed with TBST, incubated with HRP-conjugated secondary antibody for 1 h at room temperature and washed with TBST. Proteins were detected with an enhanced ECL detection kit (New England Biolabs) and a chemiluminescence detector (LAS-1000, Fuji, Japan).

2.4. Determination of cell volume

The volume of nontreated cells was determined by calculating sphere volumes based on diameter measurement of 100 cells. Since the morphology of treated cells was not spherical, cell volume was estimated by weighing the pellet of $2–4\times10^6$ cells and evaluating the volume on the assumption of 1/1 w/v.

2.5. Assay for glutathione and free SH

Cells were collected (600 g, 7 min, 4°C), washed with PBS and the pellets were stored at −80°C. After protein precipitation with 5% metaphosphoric acid (0.2–0.3 ml/3×10^6 cells) by centrifugation (10,000g, for 30 min), the supernatant was used for GSH quantitation, and the pellet, dissolved in 0.2–0.3 ml of 0.5 M NaOH, was used for protein determination. To determine GSH in the supernatant, a glutathione assay kit (Calbiochem) was used. GSH and GSSG content were also determined by the glutathione reductase recycling assay before and after modification with 2-vinyl pyridine [35]. Samples (40 μl) were neutralized with 2 M triethanolamine (10 μl) in a 96-well plate. The reaction was started by adding 200 μl per well of 0.4 U/ml enzyme in 143 mM phosphate buffer pH 7.5 containing 0.3 mM reduced nicotinamide adenine dinucleotide phosphate, 0.6 mM DTNB and 6.25 mM EDTA. The initial rate of 5-thio-2-nitrobenzoic acid formation was monitored. Determination of GSSG was done 1 h after modification of the free SH with 9 M 2-vinyl pyridine (1 μl/well) at room temperature. Oxidized glutathione (0–6 nmol/well) served as a reference.

Total free SH content in cell extracts or in cytosolic and mitochondrial fractions (50 μl) was determined with DTNB in a 96-well plate. Samples were acidified with 5% metaphosphoric acid (50 μl/well) to stabilize the reduced state and neutralized with 2 M triethanolamine (50 μl/well). DTNB (50 μl of 1 mM solution in 50 mM phosphate buffer pH 7.2 containing 2 mM EDTA) was added. After 10 min of incubation, the absorbance was measured at 412 nm using an ELISA reader. GSH (0–20 nmol/well) precalibrated with DTNB served as a reference, using E_M 14150 M^{-1} at 412 nm [36]. Reduction potential was calculated by using the Nernst equation for GSSG/2GSH: $E_{GSH}=E_0-30\times\log([GSH]^2/[GSSG])$ [27].

2.6. Statistical analysis

Each experiment was performed at least three times, and the results were expressed as mean values± S.D. (n=2–6). The Student t test was used to determine the significance of differences between the mean values obtained for the two cell lines. Otherwise, the various treatments, were analyzed using one-way analysis of variance (ANOVA) followed by either Dunnett or Bonferroni's multiple comparison test, considering $P<.05$ as significant.

3. Results

3.1. Allicin inhibited proliferation of HL60 and U937 cells

The proliferation rate of exponentially growing HL60 and U937 cells in the presence of allicin was determined at a density of 100,000 cells ml^{-1}. Cells were incubated with increasing concentrations of allicin (HL60: 0–10 μM; U937: 0–30 μM) for growing time periods up to 72 h. Cell viability was determined by the trypan blue dye exclusion assay. Allicin inhibited cell growth in a concentration-dependent manner (Figs. 1A and 2A for HL60 and U937, respectively). In the presence of 5 μM allicin, HL60 cells exhibited about 50% inhibition of proliferation after 22 h, and at 10 μM allicin after 22 h, the rate of inhibition reached 80% (Fig. 1A). HL60 cells were more sensitive to allicin than U937 cells. Inhibition of U937 cell proliferation reached 50% and 60% at 15 and 20 μM allicin, respectively, after 22 h (Fig. 2A). We therefore chose to continue the study of HL60 and U937 cells (100,000 cells/ml) at 5 and 20 μM allicin, respectively.

3.2. Allicin induced apoptosis in the cells

3.2.1. Morphological changes

Morphological changes indicating apoptotic processes were observed by staining the cells with Hoechst 33342. Distinct nuclear condensation was observed in HL60 cells treated with allicin (5 μM) for 16 h (Fig. 1B) and U937 cells treated with allicin (20 μM) for 40 h (Fig. 2B). In both allicin-treated cell lines, more than 90% of the cells showed blebbing after 2 h (Fig. 3A, lower panel).

3.2.2. DNA fragmentation

A DNA ladder appeared in allicin (5 μM)-treated HL60 cells 6 h after treatment, whereas in allicin (20 μM)-treated U937 cells, it appeared only after 40 h (Figs. 1C and 2C).

3.2.3. Cytochrome c release into cytoplasm and activation of caspases

To better understand the mechanism of allicin-induced apoptosis, Western blot analysis was used to detect apoptosis-related proteins. Increased amounts of cytochrome *c* appeared in the cytosol of allicin (5 μM)-treated HL60 cells after 2.5 h of incubation. An increase in cleaved caspase 9 appeared 4 and 6 h after adding allicin, and it gradually decreased to the basal level after 30 h. Cleaved caspase 3 appeared after 16 h and was still observed 30 h after the treatment (Fig. 3B). U937 cells reacted at a slower rate to allicin (20 μM) treatment. Cytochrome *c* release into the cytosol began 6 h after adding allicin and reached a maximal

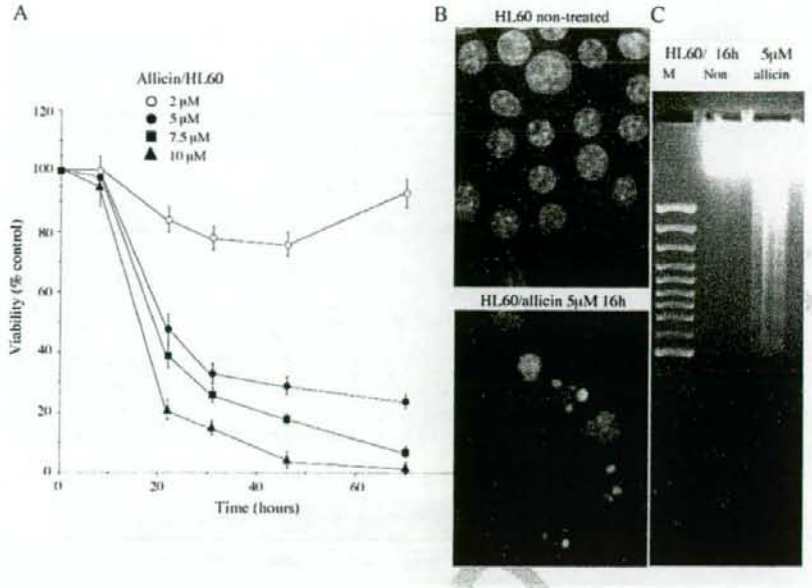

Fig. 1. Effect of allicin on cell growth of human leukemia HL60 cells. (A) Growth dependent of HL60 cells on allicin concentration. Viable cells were counted at various time intervals between 0–72 h after staining with trypan blue. Data represent the mean value of % viable cells (nontreated=100%)±S.D. (B) Apoptotic changes observed after Hoechst 33342 (5 μg/ml) staining for 30 min. Cells were treated with 5 μM allicin for 16 h. (C) Nucleosomal DNA fragmentation of nontreated cells and allicin-treated HL60 cells (5 μM, 6 h, 5 μg/lane). Lane M is a DNA size marker.

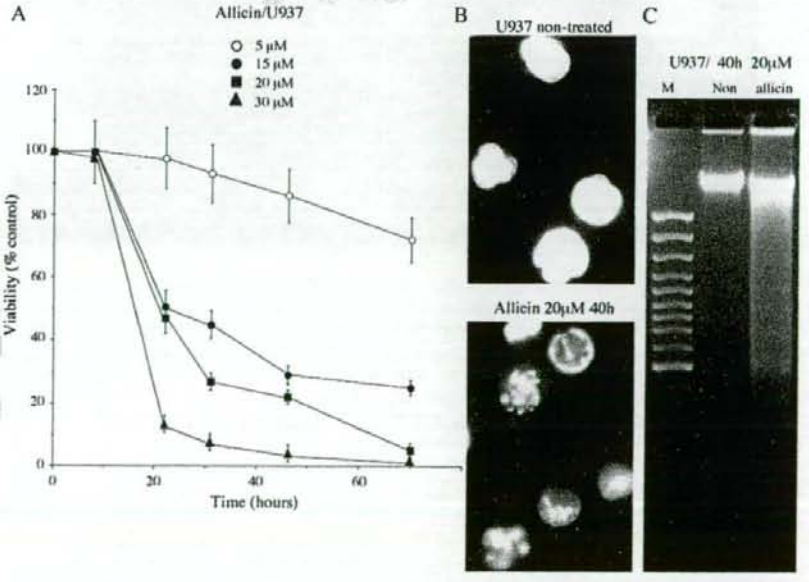

Fig. 2. Effect of allicin on cell growth of human leukemia U937 cells. (A) Growth dependence of U937 cells on allicin concentration. Viable cells were counted at various time intervals between 0–72 h after staining with trypan blue. Data represent the mean value of % viable cells (nontreated=100%)±S.D. (B) Hoechst 33342 (5 μg/ml) staining for 30 min of cells treated with 20 μM allicin for 40 h. (C) Nucleosomal DNA fragmentation of nontreated cells and allicin-treated U937 cells (20 μM, 40 h, 10 μg/lane). Lane M is a DNA size marker.

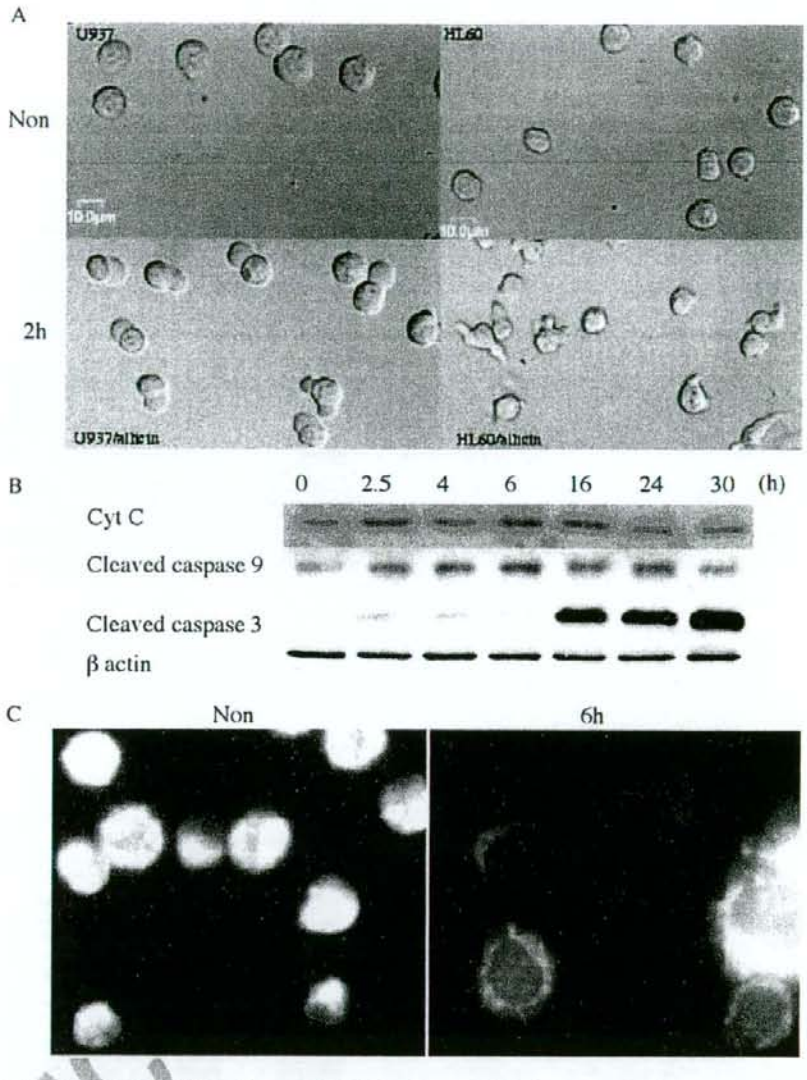

Fig. 3. (A) Morphological changes in HL60 and U937cells treated with allicin. HL60 and U937 cells treated with allicin (5 or 20 μM, respectively) for 2 h were collected and washed with PBS. Cells were visualized by confocal microscopy (original magnification ×40). (Upper panel) Nontreated cells (the diameter of 100 cells was measured). (Lower panel) Allicin-treated cells. (B) Immunoblot analysis of extracts (20 μg protein/lane) from allicin treated HL60 cells at various time of allicin (5 μM) treatment. The degrees of cytochrome *c* release into the cytosol and of caspase 9 and caspase 3 activation were assessed. β-Actin served as a control to the amount of loaded protein. The analysis of caspase 3, 9 and β-actin was done on the same blot after stripping. The data were obtained from one representative experiment (total of three independent experiments). (C) Staining of HL60 cells with MitoTracker Red CMXRos. HL60 cells treated with allicin (5 μM, 6 h) were collected, resuspended in fresh medium and were stained for 30 min with MitoTracker Red CMXRos (0.05 μM, 30 min). After washing twice with PBS, cells were examined by fluorescence microscopy (original magnification ×40).

level after 18 h. The band of cleaved caspase 9 appeared at 24 h, reached a maximal intensity at 48 h and was still seen at 72 h. Cleaved caspase 3 appeared at 30 h, became intense at 48 h and did not fade after 72 h (data not shown). Cleaved caspase 8 was not observed in either cell line after allicin treatment (data not shown).

3.2.4. Impaired mitochondrial activity

Mitochondrial activity was monitored with the XTT assay in cells treated with allicin (5 and 20 μM for HL60 and U937, respectively) for 16 h (Fig. 4). Both cell lines behaved similarly, showing a residual mitochondrial activity 65±5% in HL60 and 62±5% in U937 cells. At

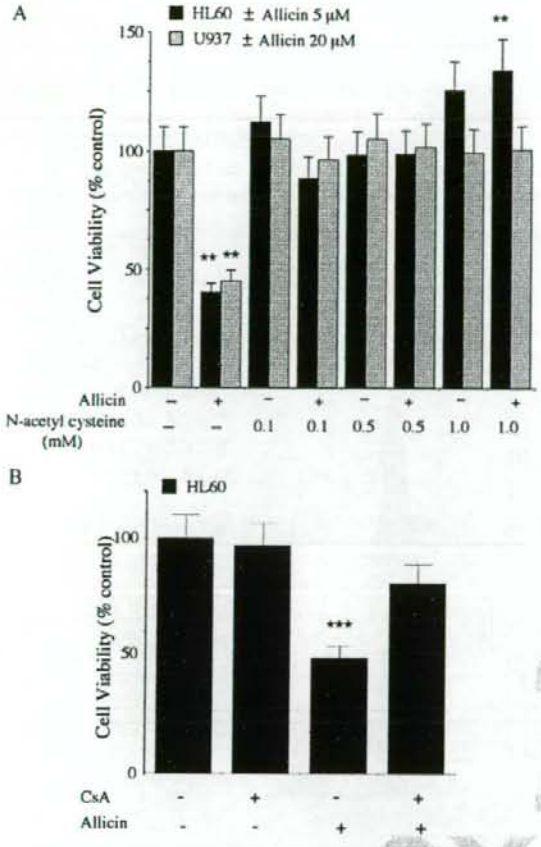

Fig. 4. (A) Allicin effect on cell viability in the absence or presence of *N*-acetyl cysteine. HL60 and U937 cells (100,000 cells/ml) were treated with allicin (5 or 20 μM, respectively) for 16 h, in the absence or presence of *N*-acetyl cysteine at 0.1, 0.5 and 1.0 mM. Cell viability was measured by the XTT assay after 3 h of incubation at 37°C with 5% CO_2. Means±S.D. of one experiment (n=6) are shown (total of three independent experiments). **P<.01 represents a significant difference from nontreated cells, based on one-way ANOVA followed by Dunnett's test. (B) Allicin effect on HL60 cell viability following a 1-h CsA (5 μM) pretreatment. HL60 cells (100,000 cells/ml) were treated with or without allicin (5 μM) for 16 h. Cell viability was measured by the XTT assay. Means±S.D. of one experiment (n=6) are shown (total of three independent experiments). ***P<.001, represents significant difference compared with nontreated cells by one-way ANOVA followed by Bonferroni's multiple comparison test.

this stage, the drop in mitochondrial activity was not accompanied by a significant change in cell number. Such a change was observed only after 24 h. Nontreated HL60 cells proliferated at a higher rate than nontreated U937 cells. Although after 24 h nontreated HL60 cells exceeded nontreated U937 cells in number, mitochondrial activity (measured by XTT assay) in U937 cells (0.869±0.025 OD units at 450 nm, n=6) was significantly higher than that in HL60 cells (0.498±0.073 OD units, n=6) (P<.001). These results indicate a higher battery of mitochondrial enzymes in U937 cells and suggest a higher resistance to allicin. When cells were treated with allicin in the presence of NAC (0.1–1.0 mM), mitochondrial metabolic activity was not impaired, and the antiproliferative effect of allicin was precluded (Fig. 4A).

3.3. Allicin induces changes in mitochondrial membrane potential

Nontreated cells showed strong staining with MitoTracker Red CMXRos, indicating the negative membrane potential of the mitochondria and the accumulation of the lipophilic dye. In HL60 cells treated with allicin (5 μM, 6 h the staining intensity decreased significantly, indicating changes in the mitochondrial membrane potential (Fig. 3C). Reduced mitochondrial staining in allicin-treated (20 μM) U937 cells occurred much slower; changes were observed 24 h after treatment, and the decline continued up to 40 h (data not shown).

A deeper insight into the involvement of mitochondrial permeability transition pore (mPTP) in the cytotoxicity of allicin was gained by using cyclosporine A (CsA), an inhibitor of adeninenucleotide translocator. HL60 cells were preincubated with 5 μM CsA for1 h and then treated with allicin for 16 or 20 h. CsA inhibited the detrimental effects of allicin on cell viability as determined by the XTT assay (~80% residual viability for CsA pretreatment; ~50% for allicin alone). There was no significant difference between nontreated and CsA-treated cells (P>.05). No significant difference was found between CsA alone and CsA followed by allicin treated cells (P>.05) (Fig. 4B). CsA-pretreated cells were stained with Hoechst 33342 and MitoTracker Red CMXRos. CsA pretreatment prevented the nuclear condensation induced by treatment with allicin alone (Fig. 5). Mitochondrial staining also showed the preventive effect of CsA, whereby allicin-induced mitochondrial membrane depolarization was inhibited.

FACS analysis of HL60 cells treated with allicin (5 μM, 20 h) showed that 35.0% of the cells were apoptotic, whereas CsA pretreatment reduced the apoptotic fraction to 17.1% (P<.05). Cell arrest at G2 was increased in allicin-treated cells with or without CsA pretreatment — 34.9% and 59.0%, respectively (Fig. 6). The fraction of HL60 cells at the G2 stage was 17.3% for nontreated cells and 18.9% for cells treated with CsA only (the difference is not significant).

3.4. Differences in GSH levels between HL60 and U937

GSH concentrations (nmol/total cell volume) in nontreated HL60 and U937 cells were almost the same: 3.4±0.48 mM and 3.7±0.55 mM, respectively. However, due to the differences in cell size between the two cell lines, analysis of GSH concentration expressed as a function of protein levels or cell numbers was also used. This analysis revealed significant differences between the GSH concentrations in the two cell lines. In nontreated HL60 cells, GSH concentration was 20.94±3.15 nmol/mg protein, and in nontreated U937 cells, 30.80±6.04 nmol/mg protein (P<.02). The

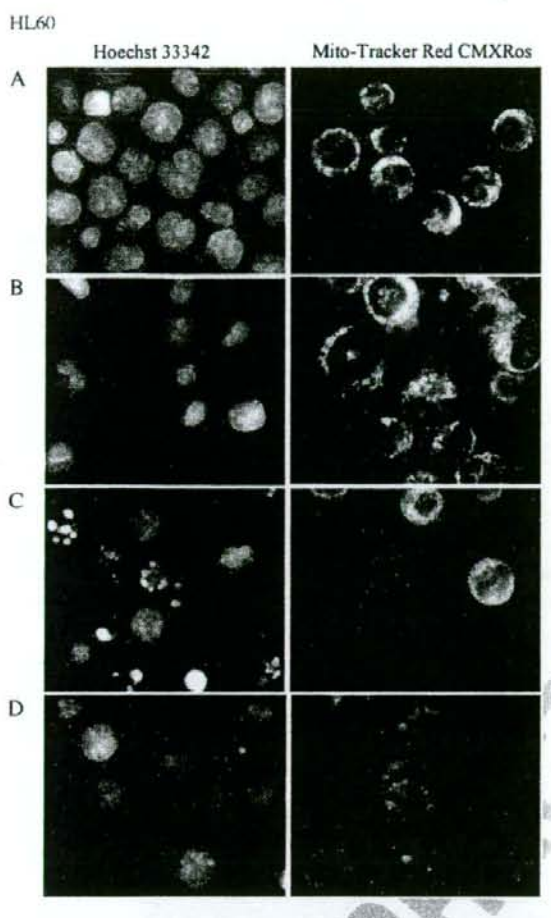

Fig. 5. Morphological effects of allicin on CsA pretreated HL60 cells. Cells (200,000 cells/ml) with or without CsA pretreatment (5 μM, 1h) were diluted and incubated in the presence or absence of allicin (5 μM) for 16 h. Cells were stained with Hoechst 33342 (5 μg/ml) or with Mito-Tracker Red CMXRos (50 nM) for 30 min. Cells were washed twice with PBS and examined by fluorescence microscopy. (A) HL60 nontreated. (B) CsA-treated. (C) Allicin-treated. (D) CsA- and allicin-treated.

difference was found to be even higher when cell numbers were considered, GSH concentration in HL60 cells was 3.7±0.56 nmol/10^6 cells whereas, in U937 cells, approximately twice as much [7.7±1.08 nmol/10^6 cells (P<001)].

3.5. Allicin-induced GSH depletion

Allicin treatment of HL60 cells caused a rapid decrease in GSH concentration, reaching its lowest point at about 30 min. A spontaneous recovery occurred, reaching the basal level of GSH (Fig. 7A). The highest GSH levels were observed in HL60 cells between 2–24 h after adding allicin. In allicin-treated U937 cells, a decrease in GSH levels to a minimal value occurred 2–4 h after treatment, and it was followed by a gradual increase to the basal GSH level (Fig. 7B).

3.6. Allicin-induced GSH depletion in the cells pretreated with BSO

In HL60 cells treated with BSO, an inhibitor of γ-glutamyl-cysteine synthetase (GGCS) (0.4 mM, 20 h) GSH levels decreased to 1.45±0.25 nmol/10^6 cells. No cell death was observed, but there was a slight decrease in the proliferation rate (×1.7 after 20 h as compared to ×2.1 in

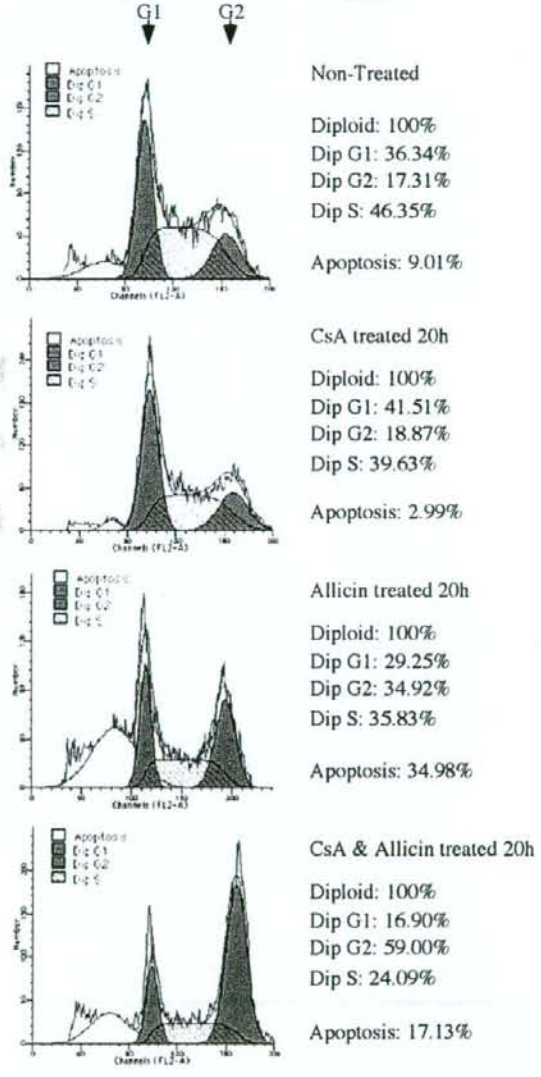

Fig. 6. Cell cycle analysis of allicin-treated HL60 cells. Cells (200,000 cells/ml, 1.5×10^6) with or without CsA pretreatment (5 μM, 1 h) were diluted and incubated in absence or presence of allicin (5 μM) for 20 h. The cells were stained with propidium iodide in the presence of RNase A and Triton X-100, as described in Materials and methods. The data represent one experiment (total of three independent experiments).

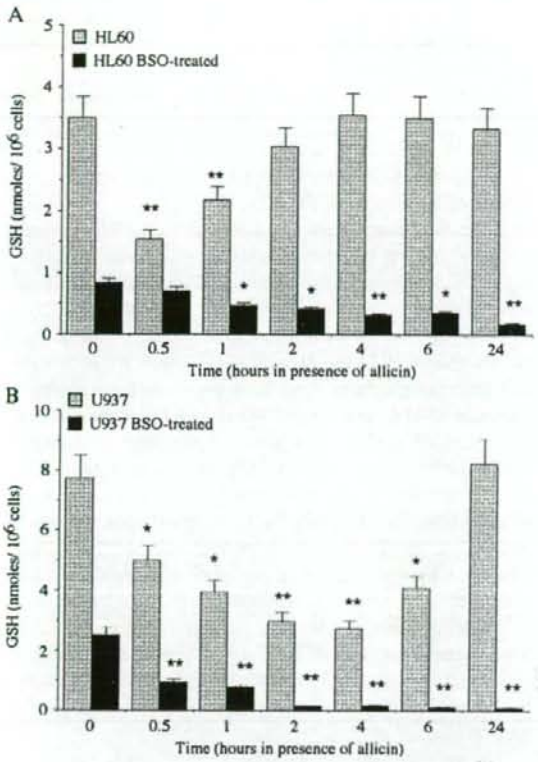

Fig. 7. Time-dependent decrease of GSH levels in allicin-treated HL60 and U937 cells after BSO pretreatment. Cells were pretreated with or without 0.4 mM BSO for 20h. HL60 and U937 cell cultures were diluted to 100,000 cells/ml and were grown in the presence of allicin (5 and 20 μM, respectively). At each time point, 30-ml samples were harvested and washed twice with PBS. Cell pellets were extracted with 5% metaphosphoric acid and analyzed for GSH content and protein concentration. Means±S.D. of one representative experiment (total of three independent experiments).

nontreated cells). Allicin (5 μM) applied to HL60 cells pretreated with BSO (0.4 mM, 20 h) caused an additional GSH decrease to 0.65±0.13 nmol/10^6 cells after 1 h (Fig. 7A, black column). There was no recovery of GSH as in the case of HL60 cells treated with allicin alone. In U937 cells pretreated with BSO (0.4 mM, 20 h), GSH levels decreased to 1.06±0.14 nmol/10^6 cells. Also, in this case, no cell death was observed and cells were still proliferating. When BSO-pretreated U937 cells were incubated with allicin (20 μM), GSH levels further decreased to 0.33±0.08 nmol/10^6 cells within 2 h (Fig. 7B, black column). A high rate of cell death (60–80%) occurred in both cell lines 24 h after allicin was applied to the culture.

3.7. Reduction potential in allicin-treated cells

Since allicin-treated cells lost their spherical structure and their volume could not be calculated from diameter measurement, we had to use another parameter to calculate changes in the intracellular reducing state resulting from fluctuations in 2GSH/GSSG ratios. Based on the assumption that 1-mg cell pellet is equivalent to 1 μl of volume, cell pellets were weighed, and GSH molar concentration was calculated accordingly (GSH amount/cell weight). Therefore, calculated reduction potential represents only approximate values. The intracellular pH of HL60 cells is 7.0 [37], and the reported E_0 for this pH is −240 mV [27]. Using the above E_0 values, reducing potential (E_{GSH}) calculated for nontreated HL60 was −207 mV (GSH 3.42±0.18 mM, GSSG 0.15±0.023 mM) and for allicin-treated (0.5 h) −169 mV (GSH 1.4±0.17 mM, GSSG 0.46±0.082 mM). The intracellular pH of U937 cells is 7.04 [38] or 7.2 [39], and the

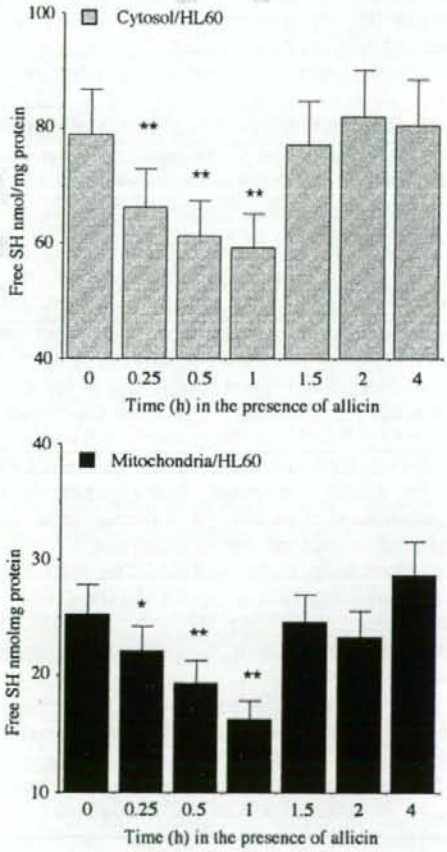

Fig. 8. Free SH contents in cytosolic and crude mitochondrial fractions from allicin-treated HL60 cells. Allicin (5 μM) was added to cells growing at density of 100,000 cells/ml. At various intervals, 100-ml samples were harvested at 4°C, washed twice with PBS and stored at −80°C overnight. Cell fractionation was done as described in Materials and methods. Total free SH and protein concentrations were determined as described in Materials and methods. The SH content at various time intervals in the cytosol (upper panel) and in the crude mitochondrial fraction (lower panel) are shown. Means±S.D. of one representative experiment (total of three independent experiments) [40].

reported E_0 values are −240 mV or −252 mV, respectively. The calculated reducing potential values of nontreated U937 cells were −206 mV or −218 mV (GSH 3.7±0.21 mM, GSSG 0.18±0.040 mM), and for allicin-treated cells (2 h), −173 mV or −185 mV (GSH 1.54±0.042 mM, GSSG 0.41±0.021 mM). The values obtained for nontreated cells are characteristic of cells in proliferation/differentiation state, whereas those obtained after allicin treatment are typically obtained in the apoptotic state.

3.8. Free SH in the cytosolic and mitochondrial fractions of HL60 cells

Total free SH concentrations were determined in the cytosol and in the crude mitochondrial fractions prepared from allicin-treated HL60 cells. The decrease in free SH in the cytosol (Fig. 8, upper panel) was accompanied by a decrease of free SH in the mitochondria (Fig. 8, lower panel). Since mitochondrial GSH is supplied from the cytoplasm and upon allicin treatment it was depleted in both cellular compartments, it was followed by a substantial decrease in the cell-reducing potential. Consequently, depolarization of the mitochondrial membrane occurred and triggered a chain of apoptotic events leading to cell death.

4. Discussion

GSH, cysteine and accessible free SH groups of various proteins and peptides are rapidly oxidized by allicin to their respective allyl-SS derivatives [19,22]. The mixed disulfide formed is less active than allicin, yet it can easily react with free SH in thiol-disulfide exchange reactions, and produce, at the end of a series of reactions, the oxidized form of glutathione (GSSG), the oxidized form of cysteine (cystine) and glutathiolated S proteins. The leaving group (allyl-mercaptan) is volatile and rapidly disappears.

Glutathione is the major regulator of the thiol-disulfide redox state of living cells (reviewed in Refs. [29,41–43]). Alterations in cellular free thiols have already been described as a key event in the generation of apoptosis (reviewed in [44,45]).

In this study, allicin induced mitochondrial release of cytochrome *c*, activation of caspase 9 and 3 and DNA fragmentation in HL60 and U937 cell lines in a concentration- and time-dependent manner. GSH depletion had been shown to be associated with cell surface blebbing in hepatocytes [46]. Here, cell blebbing occurred in both HL60 and U937 cells treated with allicin. The rate of free SH depletion from the cytosol and the mitochondria was similar, indicating that allicin penetrated the mitochondria and the cell membrane equally well and reacted with free SH in both compartments. Allicin induced an initial drop in GSH levels that was followed by a regeneration process, occurring several hours after treatment. This may be due to decreased feedback inhibition of GSH biosynthetic enzymes such as GGCS by GSH [45]. Conversely, in BSO-pretreated cells, there was no recovery of GSH after its allicin-induced depletion, as BSO is a direct inhibitor of GGCS. BSO pretreatment in allicin-treated U937 cells shortened the life span from 72 to 20 h, indicating that preliminary GSH depletion renders cells more sensitive to apoptosis. BSO-depleted GSH levels in U937 cells were, at this stage, similar to the inherent GSH level in HL60 cells and, hence, a similar degree of sensitivity to allicin.

Here, we have shown that allicin causes GSH depletion concomitantly in the cytosol and the mitochondria in HL60 cells. It is known that active GSH uptake by intact mitochondria occurs even at very low cytosolic GSH levels and that the rate of mitochondrial GSH depletion is much slower than that of the cytosol [47]. These are indications that mitochondria have more than one control mechanism to maintain GSH levels. Since BSO-induced depletion of GSH levels caused neither mitochondrial permeability transition nor apoptosis, it is likely that BSO treatment depletes GSH mainly from the cytosol, whereas allicin induced depletion of mitochondrial GSH trigger the apoptotic process. Moreover, CsA (mPTP inhibitor) pretreatment of HL60 cells inhibits allicin-induced mitochondrial permeability transition and cell death, corroborating the central role of mitochondria in the apoptotic process induced by allicin. Simultaneous addition of NAC and allicin to cells provided protection against the apoptotic damage. NAC sequestered the harmful activity by competing with GSH for the reaction with allicin.

The following allicin-induced apoptotic scenario can be deduced from this study: Allicin penetrates the cells and readily reacts with any exposed SH present in its vicinity. As GSH is the most abundant thiol molecule in the cytosol and the mitochondria, it is the main target for allicin reaction. The reaction with glutathione leads to an immediate change in the ratio GSH/GSSG. The increased concentration of GSSG and the depletion of GSH brings about a decrease in the cellular reduction potential state. Concomitantly, mitochondrial damage occurs, as is evident from changes in membrane potential, its decreased enzymatic activity and the release of cytochrome *c* to the cytosol. Upon its release, cytochrome *c* participates in the activation of the caspase 9, followed by activation of caspase 3.

Allicin induced cell cycle arrest at G2/M in HL60 cells (~35%). Upon CsA pretreatment, the percentage of cells at G2/M was even higher (~59%). After pretreatment of HL60 cells with CsA and 40-h incubation with allicin, there was no change in the number of viable cells, neither were there signs of cell breakage. By using CsA, it could be shown that the effect of allicin on cell cycle arrest was independent of its proapoptotic activity. The mechanism by which allicin induces G2/M cell arrest is not clear, but a clue may reside in its ability to inhibit microtubule assembly. It had been shown that microtubule assembly is disrupted by direct modification of tubulin SH groups [48–50] and that adding GSH to an in vitro microtubule assembly system disrupted by SH modification restores tubulin polymerization [51].

Here we have shown that, in allicin-treated cells, there is an increase in GSH synthesis. Therefore, cell cycle arrest would be expected to expire after tubulin recovery. However, the protracted G2/M phase induced by cyclosporine A and allicin suggests an additional modification of a critical pathway that needs an extended period to regenerate.

Allicin disappears from the medium very rapidly due to its penetration into the cells and its reaction with SH group. When applied to HL60 cells (5 $\mu M/10^5$ cells/ml) or to U937 cells (20 $\mu M/10^5$ cells/ml), it could not be detected in the medium after 2 h or 6–8 h in HL60 or U937 cells, respectively. The consumption of allicin within such a short time enables full activity of SH-dependent apoptotic enzymes such as the cysteine proteases and caspases 9 and 3 [52].

Cell sensitivity to allicin was shown to be dependent on the intracellular content of GSH. Since there is a significant difference in cell size between the two cell lines examined, comparing GSH amount/cell number showed that HL60 cells contained 3.7 nmol GSH/10^6 cells, whereas U937 cells contained 7.7 nmol GSH/10^6 cells. The differences in GSH intracellular content reflect differences in sensitivity to allicin. The higher the GSH, the less sensitive to allicin cells are, and the slower the apoptotic signs appear.

The allicin-induced decrease in GSH levels modulates the redox state of cells. In allicin-treated HL60 cells, the ratio of [GSH]/[GSSG or GSSA] changed within the first 30 min and the reducing potential reached −170 mV, whereas in U937 cells, it took 2 h to reach the same level. Such a high value is typical of the apoptotic state [27].

Since GSSA (the first main product of allicin reaction with GSH) is able to prevent the formation of free radicals [19], it is likely that the initial event inducing apoptosis does not occur via the generation of reactive oxygen species but rather through mitochondrial membrane depolarization or through a more finely tuned event mediated by protein modification upon creating a mixed disulfide [19,53]. Oxidative stress incurred by the accumulation of peroxides is a secondary event probably happening after the short-lived GSSA is eliminated from the cells.

It was reported that, in BSO-treated U937 cells, the depletion of GSH and the release of cytochrome *c* into the cytosol were counteracted by cell-repair systems involving nuclear factor κB and heat shock proteins [54]. Our results show that CsA and NAC prevented apoptosis induced by allicin. Taken together, the role allicin plays may be through direct modification of specific free SH in proteins, such as reside in apoptotic repair system, in the mPTP [55] or others.

Acknowledgement

We would like to thank Dr. A. Gross, Department of Biological Regulation, Weizmann Institute of Science for critical reading of the manuscript, and Mrs. Anna Gakamsky for her help in the statistical analysis.

References

[1] Stoll A, Seebeck E. Chemical investigation on alliin, the specific principle of garlic. Adv Enzymol 1951;11:377–400.

[2] Koch HP, Lawson LD. Garlic: the Science and therapeutic application of *Allium sativum* L. and related species2nd ed. 1996 [Baltimore].

[3] Elkayam A, Mirelman D, Peleg E, Wilchek M, Miron T, Rabinkov A, et al. The effects of allicin and enalapril in fructose-induced hyperinsulinemic hyperlipidemic hypertensive rats. Am J Hypertens 2001;14:377–81.

[4] Eilat S, Oestraicher Y, Rabinkov A, Ohad D, Mirelman D, Battler A, et al. Alteration of lipid profile in hyperlipidemic rabbits by allicin, an active constituent of garlic. Coron Artery Dis 1995;6:985–90.

[5] Abramovitz D, Gavri S, Harats D, Levkovitz H, Mirelman D, Miron T, et al. Allicin-induced decrease in formation of fatty streaks (atherosclerosis) in mice fed a cholesterol-rich diet. Coron Artery Dis 1999; 10:515–9.

[6] Gonen A, Harats D, Rabinkov A, Miron T, Mirelman D, Wilchek M, et al. The antiatherogenic effect of allicin: possible mode of action. Pathobiology 2005;72:325–34.

[7] Lang A, Lahav M, Sakhnini E, Barshack I, Fidder HH, Avidan B, et al. Allicin inhibits spontaneous and TNF-alpha induced secretion of proinflammatory cytokines and chemokines from intestinal epithelial cells. Clin Nutr 2004;23:1199–208.

[8] Agarwal KC. Therapeutic actions of garlic constituents. Med Res Rev 1996;16:111–24.

[9] Hirsch K, Danilenko M, Giat J, Miron T, Rabinkov A, Wilchek M, et al. Effect of purified allicin, the major ingredient of freshly crushed garlic, on cancer cell proliferation. Nutr Cancer 2000;38:245–54.

[10] Knowles LM, Milner JA. Possible mechanism by which allyl sulfides suppress neoplastic cell proliferation. J Nutr 2001;131:1061S–6S.

[11] Sun L, Wang X. Effects of allicin on both telomerase activity and apoptosis in gastric cancer SGC-7901 cells. World J Gastroenterol 2003;9:1930–4.

[12] Oommen S, Anto RJ, Srinivas G, Karunagaran D. Allicin (from garlic) induces caspase-mediated apoptosis in cancer cells. Eur J Pharmacol 2004;485:97–103.

[13] Park SY, Cho SJ, Kwon HC, Lee KR, Rhee DK, Pyo S. Caspase-independent cell death by allicin in human epithelial carcinoma cells: involvement of PKA. Cancer Lett 2005;224:123–32.

[14] Antlsperger DSM, Dirsch VM, Ferreira D, Su JL, Kuo ML, Vollmar AM. Ajoene-induced cell death in human promyeloleukemic cells does not require JNK but is amplified by the inhibition of ERK. Oncogene 2003;22:582–9.

[15] Jin Z, El-Deiry WS. Overview of cell death signaling pathways. Cancer Biol Ther 2005;4:139–63.

[16] Hsu YT, Wolter KG, Youle RJ. Cytosol-to-membrane redistribution of Bax and Bcl-XI during apoptosis. Proc Natl Acad Sci U S A 1997;94:3668–72.

[17] Wolter KG, Hsu YT, Smith A, Nechushtan A, Xi X, Youle RJ. Movement of Bax from the cytosol to mitochondria during apoptosis. J Cell Biol 1997;139:1281–92.

[18] Miron T, Rabinkov A, Mirelman D, Wilchek M, Weiner L. The mode of action of allicin: its ready permeability through phospholipid membranes may contribute to its biological activity. Biochim Biophys Acta 2000;1463:20–30.

[19] Rabinkov A, Miron T, Mirelman D, Wilchek M, Glozman S, Yavin E, et al. *S*-allylmercaptoglutathione: the reaction product of allicin with glutathione possesses SH-modifying and antioxidant properties. Biochim Biophys Acta 2000;1499:144–53.

[20] Xiao H, Parkin KL. Antioxidant functions of selected allium thiosulfinates and *S*-alk(en)yl-L-cysteine sulfoxides. J Agric Food Chem 2002;50:2488–93.

[21] Okada Y, Tanaka K, Sato E, Okajima H. Kinetic and mechanistic studies of allicin as an antioxidant. Org Biomol Chem 2006;4:4113–7.

[22] Rabinkov A, Miron T, Konstantinovski L, Wilchek M, Mirelman D, Weiner L. The mode of action of allicin: trapping of radicals and

interaction with thiol containing proteins. Biochim Biophys Acta 1998;1379:233–44.
[23] Freeman F, Kodera Y. Garlic chemistry-stability of *S*-(2-propenyl) 2-propene-1-sulfinothioate (allicin) in blood, solvents, and simulated physiological fluids. J Agric Food Chem 1995;43:2332–8.
[24] Lachmann G, Lorenz D, Radeck W, Steiper M. The pharmacokinetics of the S35 labeled garlic constituents alliin, allicin and vinyldithiine. Arzneimittelforschung 1994;44:734–43.
[25] Miron T, Mironchik M, Mirelman D, Wilchek M, Rabinkov A. Inhibition of tumor growth by a novel approach: in situ allicin generation using targeted alliinase delivery. Mol Cancer Ther 2003; 2:1295–301.
[26] Arditti F, Rabinkov A, Miron T, Reisner Y, Berrebi A, Wilchek M, et al. Apoptotic killing of B-chronic lymphocytic leukemia tumor cells by allicin generated in situ using a rituximab–alliinase conjugate. Mol Cancer Ther 2005;4:325–31.
[27] Schafer FQ, Buettner GR. Redox environment of the cell as viewed through the redox state of the glutathione disulfide/glutathione couple. Free Radic Biol Med 2001;30:1191–212.
[28] Jonas CR, Ziegler TR, Gu LH, Jones DP. Extracellular thiol/disulfide redox state affects proliferation rate in a human colon carcinoma (Caco2) cell line. Free Radic Biol Med 2002;33:1499–506.
[29] Gilbert HF. Molecular and cellular aspects of thiol-disulfide exchange. Adv Enzymol Relat Areas Mol Biol 1990;63:69–172.
[30] Stoll A, Seebeck E. Allium compounds V. The synthesis of natural alliin and its three optical active isomers. Helv Chim Acta 1951;34: 481–7.
[31] Miron T, SivaRaman H, Rabinkov A, Mirelman D, Wilchek M. A method for continuous production of allicin using immobilized alliinase. Anal Biochem 2006;351:152–4.
[32] Nakagawa Y, Iinuma M, Matsuura N, Yi K, Naoi M, Nakayama T, et al. A potent apoptosis-inducing activity of a sesquiterpene lactone, arucanolide, in HL60 cells: a crucial role of apoptosis-inducing factor. J Pharmacol Sci 2005;97:242–52.
[33] Grinberg M, Schwarz M, Zaltsman Y, Eini T, Niv H, Pietrokovski S, et al. Mitochondrial carrier homolog 2 is a target of tBID in cells signaled to die by tumor necrosis factor alpha. Mol Cell Biol 2005;25: 4579–4590.
[34] Gornall A, Bardawill C, David M. Determination of serum proteins by means of the biuret reaction. J Biol Chem 1949;177:751–66.
[35] Anderson ME. Determination of glutathione and glutathione disulfide in biological samples. Methods Enzymol 1985;113:548–55.
[36] Riddles PW, Blakeley RL, Zerner B. Ellman's reagent: 5,5′-dithiobis (2-nitrobenzoic acid) — a reexamination. Anal Biochem 1979;94: 75–81.
[37] Restrepo D, Kozody DJ, Spinelli LJ, Knauf PA. pH Homeostasis in promyelocytic leukemic HL60 cells. J Gen Physiol 1988;92:489–507.
[38] Oehler R, Zellner M, Hefel B, Weingartmann G, Spittler A, Struse HM, et al. Influence of heat shock on cell volume regulation: protection from hypertonic challenge in a human monocyte cell line. FASEB J 1998;12:553–60.
[39] Nilsson C, Kagedal K, Johansson U, Ollinger K. Analysis of cytosolic and lysosomal pH in apoptotic cells by flow cytometry. Methods Cell Sci 2003;25:185–94.
[40] Amonkar SV, Reeves EL. Mosquito control with active principle of garlic, *Allium sativum*. J Econ Entomol 1970;63:1172–5.
[41] Powis G. Anticancer drugs acting against signaling pathways. Curr Opin Oncol 1995;7:554–9.
[42] Sies H. Glutathione and its role in cellular functions. Free Radic Biol Med 1999;27:16–21.
[43] Moran LK, Gutteridge JM, Quinlan GJ. Thiols in cellular redox signalling and control. Curr Med Chem 2001;8:763–72.
[44] Meister A. Glutathione metabolism. Methods Enzymol 1995;251:3–7.
[45] Lash LH. Mitochondrial glutathione transport: physiological, pathological and toxicological implications. Chem Biol Interact 2006;163: 54–67.
[46] Jewell SA, Bellomo G, Thor H, Orrenius S, Smith M. Bleb formation in hepatocytes during drug metabolism is caused by disturbances in thiol and calcium ion homeostasis. Science 1982;217:1257–9.
[47] Meister A. Mitochondrial changes associated with glutathione deficiency. Biochim Biophys Acta 1995;1271:35–42.
[48] Kuriyama R, Sakai H. Role of tubulin-SH groups in polymerization to microtubules. Functional-SH groups in tubulin for polymerization. J Biochem (Tokyo) 1974;76:651–4.
[49] Li M, Liu JR, Ye Y, Min JM, Zhang LH, Wang K, et al. Antitumor activity of Z-ajoene, a natural compound purified from garlic: antimitotic and microtubule-interaction properties. Carcinogenesis 2002;23:573–9.
[50] Xiao D, Pinto JT, Soh JW, Deguchi A, Gundersen GG, Palazzo AF, et al. Induction of apoptosis by the garlic-derived compound *S*-allylmercaptocysteine (SAMC) is associated with microtubule depolymerization and c-Jun NH(2)-terminal kinase 1 activation. Cancer Res 2003;63:6825–37.
[51] Nishida E, Kobayashi T. Relationship between tubulin SH groups and bound guanine nucleotides. J Biochem (Tokyo) 1977;81:343–7.
[52] Thornberry NA. Caspases: key mediators of apoptosis. Chem Biol 1998;5:R97–R103.
[53] Patya M, Zahalka MA, Vanichkin A, Rabinkov A, Miron T, Mirelman D, et al. Allicin stimulates lymphocytes and elicits an antitumor effect: a possible role of p21(ras). Int Immunol 2004;16:275–81.
[54] Filomeni G, Aquilano K, Rotilio G, Ciriolo MR. Antiapoptotic response to induced GSH depletion: involvement of heat shock proteins and NF-kappaB activation. Antioxid Redox Signal 2005; 7:446–55.
[55] McStay GP, Clarke SJ, Halestrap AP. Role of critical thiol groups on the matrix surface of the adenine nucleotide translocase in the mechanism of the mitochondrial permeability transition pore. Biochem J 2002541;367:548.

DOI 10.1007/s00702-005-0410-5
J Neural Transm (2006) 113: 633–644

Journal of Neural Transmission
Printed in Austria

Neuromelanin induces oxidative stress in mitochondria through release of iron: mechanism behind the inhibition of 26S proteasome

M. Shamoto-Nagai[1], W. Maruyama[1], H. Yi[2], Y. Akao[2], F. Tribl[3], M. Gerlach[4], T. Osawa[5], P. Riederer[3], and M. Naoi[2]

[1] Department of Geriatric Medicine, National Institute for Geriatrics and Gerontology, Obu, Aichi, and
[2] Department of Neurosciences, Gifu International Institute of Biotechnology, Kakamigahara, Gifu, Japan
[3] Clinical Neurochemistry and NPF Center of Excellence Laboratories, Department of Psychiatry and Psychotherapy, and
[4] Laboratory of Clinical Neurochemistry, Clinic for Child and Adolescent Psychiatry and Psychotherapy, University of Würzburg, Würzburg, Germany
[5] Laboratory of Food and Biodynamics, Nagoya University Graduate School of Bioagricultural Sciences, Nagoya, Aichi, Japan

Received May 15, 2005; accepted October 20, 2005
Published online December 16, 2005; © Springer-Verlag 2005

Summary. Parkinson's disease is characterized by the selective depletion of dopamine neurons in the substantia nigra, particular those containing neuromelanin. Involvement of neuromelanin in the pathogenesis may be either cytotoxic or protective. Recently we found that neuromelanin reduces the activity of 26S proteasome. In this paper, the detailed mechanisms behind the reduced activity were studied using neuromelanin isolated from the human brain. Neuromelanin increased the oxidative stress, but synthetic melanin did not. Superoxide dismutase and deferoxamine completely suppressed the increase, indicating that superoxide produced by an iron-mediated reaction plays a central role. Iron was shown to reduce *in situ* 26S proteasome activity in SH-SY5Y cells and the reduction was protected by antioxidants. These results suggest that iron released from neuromelanin increases oxidative stress in mitochondria, and then causes mitochondrial dysfunction and reduces proteasome function. The role of neuromelanin is discussed in relation to the selective vulnerability of dopamine neurons in Parkinson's disease.

Keywords: Neuromelanin, mitochondria, oxidative stress, Parkinson's disease, ubiquitin-proteasome system, ferrous iron.

Abbreviations

ACM 7-Aminomethylcoumarin; *DCF* 2′,7′-Dichlorofluorescein; *DFX* deferoxamine mesylate; *DMSO* dimethyl sulfoxide; *EGCG* (−)-epigallocatechin gallate; *GFP* green fluorescent protein; *H_2DCFDA* 2′,7′-dichlorodihydrofluorescein diacetate; *MEM* minimum essential medium; *MG132* *N*-benzoyloxycarbonyl (Z)-Leu-Leu-leucinal; *NAC* *N*-acetyl cysteine; *NM* neuromelanin; *NO*$^{\bullet}$ nitric oxide; *$O_2^{\bullet -}$* superoxide radical;

^{-}OH hydroxyl radical; *$ONOO^{-}$* peroxynitrite; *PBS* phosphate-buffered saline; *PD* Parkinson's disease; *PI* propidium iodide; *PSI* carbobenzoxy-L-isoleucyl-γ-*t*-butyl-L-glutamyl-L-alanyl-L-leucinal [Z-Ile-Glu(Obu^{t})-Ala-Leu-H (aldehyde)]; *SN* substantia nigra; *SOD* superoxide dismutase; *UP* ubiquitin-proteasome; *ZsGFP Zoanthus* sp. green fluorescence protein.

Introduction

In Parkinson's disease (PD), degeneration of dopamine neurons in the substantia nigra (SN) and accumulation of typical inclusion bodies, Lewy bodies, are characteristic pathological features. In PD, dopaminergic neurons of the SN and noradrenergic neurons of the locus coeruleus (LC) are preferentially affected (Hirsch et al., 1988). The presence of neuromelanin (NM) in these neurons suggests that NM may be involved in their vulnerability towards insults leading to cell death (Kastner et al., 1992). NM is synthesized from quinones and semiquinones produced by enzymatic or non-enzymatic oxidation of dopamine and noradrenaline in the SN and LC, respectively. The complex polymers contain also other oxidation metabolites of dopamine and L-DOPA, cysteinyl-DOPA (Odh et al., 1994), 5-S-cysteinyl-dopamine (Zhang and Dryhurst, 1994), proteinacious components and lipids (Gerlach et al., 1995; Zecca et al., 1994, 2000; Dzierzega-Lecznar et al., 2004; Fedorow et al., 2005a; Tribl et al., 2005). In addition, inorganic components, especially iron, copper and zinc are detected in NM (Bridelli et al., 1999).

The role of NM has been discussed either in a preventing or promoting way to the degeneration of nigral dopamine neurons. NM was reported to increase the vulnerability of SN neurons (Youdim et al., 1994; Offen et al., 1997), and an iron(III)-melanin complex was cytotoxic to dopaminergic neurons *in vitro* (Double et al., 2002). Increased production of reactive oxygen and nitrogen specifies (ROS, RNS) was proposed to account for the cytotoxicity of NM-metal conjugates (Ben-Shachar et al., 1991). More recently NM was reported to increase the secretion of cytokines and nitric oxide ($NO^{\bullet}$) from microglia, which might be also related to degeneration of dopamine neurons in PD (Wilms et al., 2003). On the other hand, NM has been proposed to be neuroprotective, by scavenging redox active metals (Fe, Cu and Mn), toxic metals (Cd, Hg and Pb) (Youdim et al., 1994; Zecca et al., 1994, 2002; Double et al., 2003) and other toxins, such as 1-methl-4-phenylpyrimidium ion (MPP^{+}) (D'Amato et al., 1986) and 1,2(*N*)-dimethyl-6,7-dihydroxyisoquinolinium ion, an oxidation product of *N*-methyl-(*R*)salsolinol, an endogenous dopaminergic neurotoxin (Naoi et al., 1994). In addition, NM synthesis reduces accumulation of cytotoxic quinone produced by dopamine oxidation (Sulzer et al., 2000).

In PD, oxidative stress, mitochondrial dysfunction, excitotoxicity and inflammation have been proposed to cause the cell death in nigro-striatal dopamine neurons. Mitochondrial dysfunction results in increased oxidative stress and on the other hand, ROS and RNS induce dysfunction in mitochondrial respiratory chain, suggesting that there is a complex interrelationship between the pathogenic factors. In addition, recent evidences suggest that failure of the ubiquitin-proteasome (UP) system leads to aggregation and accumulation of abnormal proteins to form the inclusion bodies and induce neuronal cell death (Leroy et al., 1998; McNaught et al., 2002a). The UP system is now considered to contribute to the etiopathogenesis of the sporadic form of PD, in addition to the familial forms (McNaught and Olanow, 2003b). Actually, the products of genes responsible for the familial parkinsonism, α-synuclein, ubiquitin carboxy-terminal hydrolase L1 (UCH-L1), and parkin were found to co-localize with proteasomal subunits in Lewy body (Ii et al., 1997; Gai et al., 2000). "Aggresomes" formed in response to the

accumulation of abnormal proteins in neurons with reduced UP system was indicated as a precursor of Lewy body in PD (McNaught et al., 2002b).

Recently, we found that NM purified from the human reduced the activity of 26S proteasome (Shamoto-Nagai et al., 2004), both directly *in vitro* and also *in situ* and reduced the protein amounts of PA700 regulatory subunit. These results may be relevant with those found in the parkinsonian substantia nigra: the reduction in the activity of 20S proteasome and also the levels of the regulatory subunit, PA700 (19S, ATPase) and α-subunit of 20S proteasome (McNaught et al., 2003a). However, the detailed mechanism underlying the inhibition remains to be clarified.

In this paper, the effects of NM on the induction of oxidative stress were studied using mitochondria prepared from SH-SY5Y cells, and their effects on the *in situ* activity of proteasome were examined using SH-SY5Y cells transfected with a green fluorescent protein targeting to 26S proteasomes (proteasome sensor vector) (Shamoto-Nagai et al., 2003). Generation of hydroxyl radical ($^{\bullet}OH$), nitric oxide ($NO^{\bullet}$) and peroxynitrite ($ONOO^{-}$) was quantitatively measured by use of 2′,7′-dichlorodihydrofluorescein diacetate (H_2DCFDA) (Crow, 1997). In addition, the effects of iron on the levels of oxidative modified protein, especially acrolein-protein conjugates were examined, the increase of which was confirmed in rotenone-induced UP system failure model (Shamoto-Nagai et al., 2003). The results are discussed in relation to the possible role of NM in the cell death in PD, especially about interaction among mitochondrial dysfunction, oxidative stress and deterioration of the UP system.

Materials and methods

Materials

2′,7′-Dichlorodihydrofluorescein diacetate (H_2DCFDA) was purchased from Molecular Probes (Eugene, OR, USA). Synthetic melanin was prepared by peroxidation of L-tyrosine with hydrogen peroxide. Deferoxamine mesylate (DFX), (−)-epigallocatechin gallate (EGCG) from green tea, and superoxide dismutase (SOD) from bovine erythrocytes were purchased from Sigma (St. Louis, MO, USA). Propidium iodide (PI) was purchased from Molecular Probes (Eugene, OR. USA). 2′,7′-Dichlorofluorescein (DCF), *N*-acetyl cysteine (NAC), L-cysteine and catalase from bovine liver, minimum essential medium (MEM) and other reagents were from Wako (Kyoto, Japan), and DL-α-tocopherol from Nacalai tesque (Kyoto, Japan). NO_2/NO_3 assay kit-F (fluorometric) was purchased from Dojindo (Kumamoto, Japan). Mouse anti-acrolein antibody was purchased from NOF (Tokyo, Japan). Inhibitors of proteasome, *N*-benzoyloxycarbonyl (Z)-Leu-Leu-leucinal (MG132) and benzyloxycarbonyl-L-isoleucyl-γ-*t*-butyl-L-glutamyl-L-alanyl-L-leucinal [PSI, Z-Ile-Glu(Obu^t)-Ala-Leu-H (aldehyde)] were purchased from Peptide Institute (Osaka, Japan). Human dopaminergic neuroblastoma SH-SY5Y cells were cultured in Cosmedium-001 tissue culture medium (CosmoBio, Tokyo, Japan), supplemented by 5% fetal calf serum in an atmosphere of 95% air and 5% CO_2.

Preparation of NM suspension

NM was isolated from the SN of neurologically normal adult individuals as previously described (Double et al., 2000). Brains were provided from the Austro-German Brain Bank in Würzburg. The use of post-mortem human brain tissue was approved by the Ethics Committee of the University Clinics of Würzburg. In brief, SN samples were homogenised in 20 ml water and centrifuged at 12 000 g for 10 min. The resulting pellets were washed twice with 50 mM phosphate buffer (pH 7.4), then incubated in 50 mM Tris buffer (pH 7.4) containing 0.5 mg · ml^{-1} SDS at 37°C for 3 h, followed by a further 3 h incubation with addition of 0.2 mg · ml^{-1} proteinase K in the same buffer. The pellets were pooled and consecutively washed with saline, water, methanol and hexane. Finally, the resulting dark pellet was incubated for three periods of 8 hrs each in 150 mM EDTA (pH 7.4) before being washed twice with water and dried under vacuum.

NM was dissolved in distilled water containing 15 mM L-cysteine and 10% dimethyl sulfoxide (DMSO) (L-Cyst-DMSO solution) to be 0.5 mg/ml in the final concentration. NM suspension was sonicated for 20 min and then shaken gently for 4 days for rehydration at room temperature under protection from light.

Isolation of mitochondria from SH-SY5Y cells

Mitochondria were prepared from SH-SY5Y cells according to Desagher et al. (1999). The cells were

gathered, washed with PBS and suspended in isotonic mitochondrial buffer (210 mM mannitol, 70 mM sucrose, 1 mM EDTA and 10 mM HEPES, pH 7.5) supplemented with complete protease inhibitor cocktail (Roche Diagnostics, Mannhein, Germany). The cells were homogenized for 20 strokes with a Dounce homogenizer, centrifuged at 500 g for 5 min, and the supernatant was centrifuged at 10 000 g for 30 min. The crude mitochondria were obtained as the pellet and suspended in PBS for following experiments.

Measurement of ROS-RNS with H_2DCFDA

The mitochondria were suspended in PBS and the production of ROS-RNS, $^{\bullet}OH$, $NO^{\bullet}$, and peroxynitrite ($ONOO^-$) produced from $NO^{\bullet}$ and superoxide ($O_2^{\bullet -}$), was quantified fluorometrically by measuring DCF produced from H_2DCFDA (Crow, 1997). H_2DCFDA was added to be 50 μM to the mitochondria suspension (20–30 μg protein in a total reaction volume of 1 ml PBS) in the presence or absence of NM suspension (1–5 μg/ml) or synthetic melanin (1–10 μg/ml) in dark at 37°C. The increase in DCF fluorescence at 504 nm with excitation at 520 nm was measured at every 30 min for 3 h in a RF-5000 spectrofluorometer (Shimadzu, Kyoto, Japan). The generation of ROS-RNS was expressed as mol DCF per min per mg protein. The effects of DFX, anti-oxidants and other agents on the increased ROS-RNS production by NM were also examined in the same way, after 15 min pre-incubation.

Assay for NO

NO is hydrolyzed into NO_2^- and NO_3^- in aqueous solution, and this assay is based on the measurement of NO_2^- with 2,3-diaminonaphthalene, which is produced by reduction of NO_3^- (Misco et al., 1993). Mitochondrial suspension (20 μg/ml) was incubated with or without NM or synthetic melanin (2.5 μg) in PBS and produced $NO^{\bullet}$ was measured according to the manufacture's instruction, and the increase in the fluorescence at 450 nm was followed with excitation at 365 nm. The amount of NO produced was quantified by comparison with the authentic NO standard, and expressed as nmol per min per mg protein.

Assay for the in situ activity of 26S proteasome, and apoptosis

To quantify the *in situ* proteasome activity, SH-SY5Y cells transfected with a proteasome sensor vector were prepared as described previously (Shamoto-Nagai et al., 2004). The vector was designed to express ZsGreen fluorescence protein (ZsGFP) fused to the degradation domain of mouse ornithine decarboxylase, a specific substrate for 26S proteasome. The reduction of 26S proteasome activity was assessed by measuring the ZsGFP fluorescence accumulated in SH-SY5Y cells transfected with the proteasome sensor vector (SH-PSV cells). SH-PSV cells were cultured in 6-well poly-L-lysine coated flasks in MEM with various concentration of iron with or without 25 μM DFX or antioxidants for 20 h. The living cells were gathered, then suspended in PBS(−). The fluorescence of the cell suspension at 505 nm with excitation at 493 nm was measured in a spectrofluorophotometer, RF-5300 (Shimadzu, Kyoto, Japan), and expressed as arbitrary fluorescence unit per mg protein. The protein amount was measured according to Bradford (1976).

At the same time SH-PSV cells were also subjected to fluorescence augmented flow cytometry (FACS) and the native fluorescence of ZsGFP was quantified. The cells were stained with 75 μM PI solution in PBS containing 1% Triton X-100 at room temperature for 5 min in the dark, washed and suspended in PBS and subjected to FACS analysis. Cells with lower DNA content showing PI staining less than G1 were defined to be apoptotic (subG1 peak) (Eckert et al., 2001).

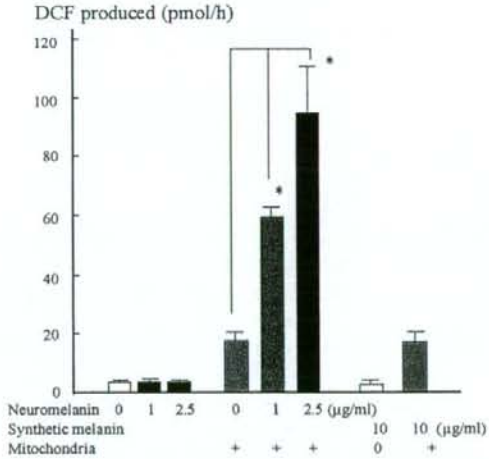

Fig. 1. ROS-RNS production in mitochondria. Mitochondria isolated from SH-SY5Y cells were incubated with or without NM or synthetic melanin. Generated ROS-RNS was quantitatively measured as DCF produced from H_2DCFDA and expressed as pmol/hr. The reaction mixture was composed of 1 ml PBS containing 0, 1, 2.5 μg human brain neuromelanin (NM) or 10 μg synthetic melanin in the presence or absence of mitochondria (28 μg protein). The column and bar represent the mean and SD of triplicate measurements of 3 independent experiments. $^*P<0.01$

Western blot analysis of acrolein-modified protein

SH-SY5Y cells were treated with 10–200 μM Fe^{2+} or Fe^{3+} in the absence or presence of 25 μM DFX for 20 h, gathered, washed with PBS, lyzed in Laemmli's sample buffer (100 mM Tris-HCl containing 4% SDS, 12% β-mercaptoethanol and 20% glycerol). The sample (20 μg protein/well) was separated by 10% polyacrylamide SDS-PAGE and blotted onto PVDF membrane, then, acrolein-modified proteins were visualized using antibody against anti-acrolein antibody, as reported (Shamoto-Nagai et al., 2003).

Statistics

Experiments were repeated at least 3 times. The data was expressed as mean ± SD and the difference was evaluated by analysis of variance (ANOVA) followed by Scheffe's F-test. A p value less than 0.05 was estimated to be statistically significant.

Results

NM increased ROS-RNS production in mitochondria

The production of $^{\bullet}OH$, NO and $ONOO^-$ in mitochondria was quantified fluorometrically using DCF cleaved from H_2DCFDA as an indicator. As shown in Fig. 1, in the presence of mitochondria, NM increased DCF fluorescence in a dose-dependent way. NM alone did not increase DCF virtually at all. On the other hand, higher amount synthetic melanin did not increase ROS-RNS levels and even in the presence of mitochondria, the increase of DCF was not significant.

Effects of DFX and anti-oxidants on ROS/RNS production by NM in mitochondria

The nature of ROS/RNS produced in mitochondria was studied by use of anti-oxidative enzymes and antioxidants. As shown in Fig. 2, SOD, but not catalase, reduced DCF production in mitochondria

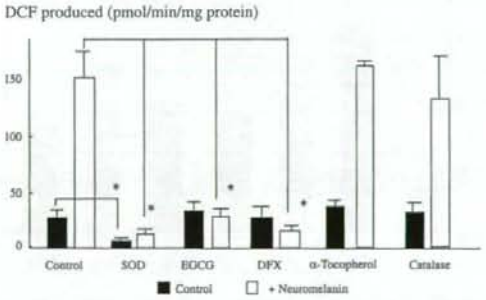

Fig. 2. Effects of SOD, (−)-epigallocatechin gallate (EGCG), deferoxamine mesylate (DFX), α-tocophenol and catalase on DCF production in mitochondria prepared from SH-SY5Y cells. Mitochondria (30 μg protein) were incubated with 2.5 μg/ml NM in PBS, and the effects of SOD (1000 units), EGCG (1 μM), DFX (1 μM), α-tocopherol (100 μM) and catalase (500 units) were examined. The column and bar represent the mean and SD of triplicate measurements of 3 independent experiments. $^*P<0.01$

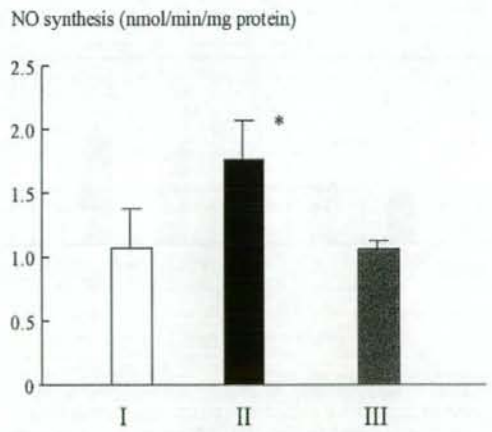

Fig. 3. Human brain neromelanin (NM) increased NO$^{\bullet}$ synthesis in mitochondria prepared from SH-SY5Y cells. NO_2^- and NO_3^- produced from NO$^{\bullet}$ were quantitatively measured with 2,3-diaminonaphthalene as an indicator, and expressed as nmol/min/mg protein. The amount of NO$^{\bullet}$ was calculated by comparing with $NO_2^{\bullet}$ standard. I: Mitochondria suspension (20 μg/ml) alone; II: mitochondria suspension incubated with NM (2.5 μg); III: mitochondria suspension incubated with synthetic melanin (2.5 μg). The column and bar represent the mean and SD of triplicate measurements of 3 independent experiments. $^*p<0.05$

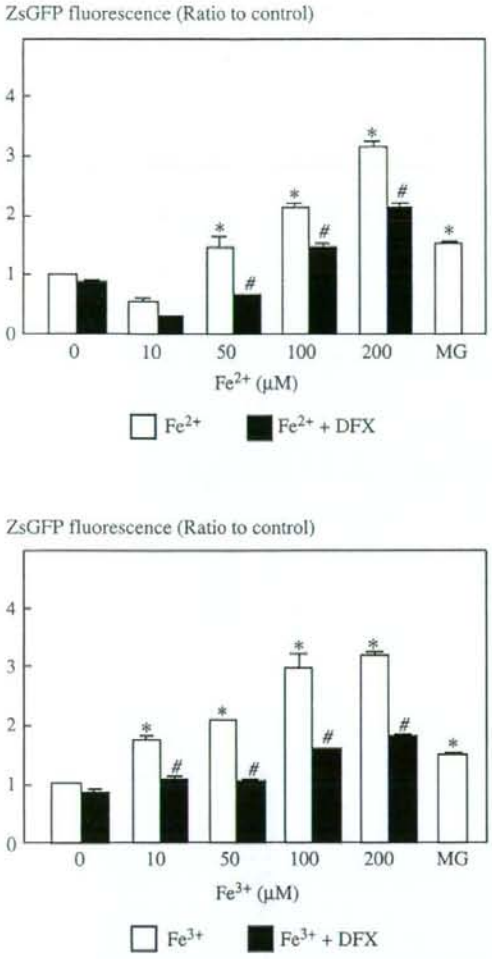

Fig. 4. Iron inhibited *in situ* activity of 26S proteasome in SH-SY5Y cells transfected with a proteasome sensor vector (SH-PSV cells). After the treatment with iron with or without deferoxamine mesylate (DFX) for 20 h, the fluorescence intensity of ZsGFP, which is coded by a proteasome sensor vetor, at 505 nm with excitation at 493 nm was quantified and expressed as arbitrary fluorescence unit/mg protein. The column and bar represent mean and SD of 3 experiments. After the treatment with iron, the fluorescence intensity increased in a dose-dependent manner. $^{*}p<0.05$ compared to the control. This increase was suppressed by 25 μM DFX significantly. $\#p<0.05$ compared to the cells treated with iron without DFX. MG; SH-PSV cells treated with 0.5 μM of MG132, a proteasome inhibitor, as a positive control

themselves. SOD, EGCG, and DFX significantly reduced the DCF production from mitochondira enhanced by NM. The reduction by SOD was most markedly, indicating that $O_2^{\cdot -}$ plays the key role in ROS-RNS production. EGCG, which preferentially scavenges NO (Akao et al., 2004), suppressed DCF production also. DFX was also potent to reduce DCF generation, suggesting the involvement of iron in the ROS-RNS production by NM. On the other hand, α-tocopherol did not affect DCF levels in mitochondria with or without NM.

Increased NO production by NM

The effects of NM and synthetic melanin on NO production were studied in mitochondria using 2,3-diaminonaphthalene as an indicator. As shown in Fig. 3, only NM increased NO level in mitochondria, whereas synthetic melanin did not affect the NO level in mitochondria.

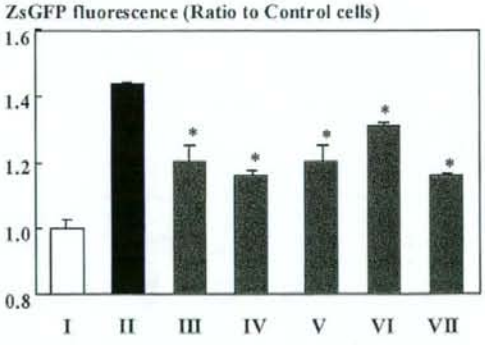

Fig. 5. Antioxidants suppressed the iron-induced inhibition of 26S proteasome activity in SH-SY5Y cells transfected with a proteasome sensor vector (SH-PSV cells). I: Control, II: treated with 100 μM Fe^{2+}, III–VII: pre-incubated with 50 μM ascorbic acid, 50 μM NAC, 0.5 μM (−)-epigallocatechin gallate (EGCG), 50 μM GSH and 50 μM of α-tocopherol, respectively for 30 min, then with Fe^{2+} for 20 h. The column and bar represent the mean and SD of 3 experiments. $^{*}p<0.05$ compared to the cells treated with Fe^{2+} alone

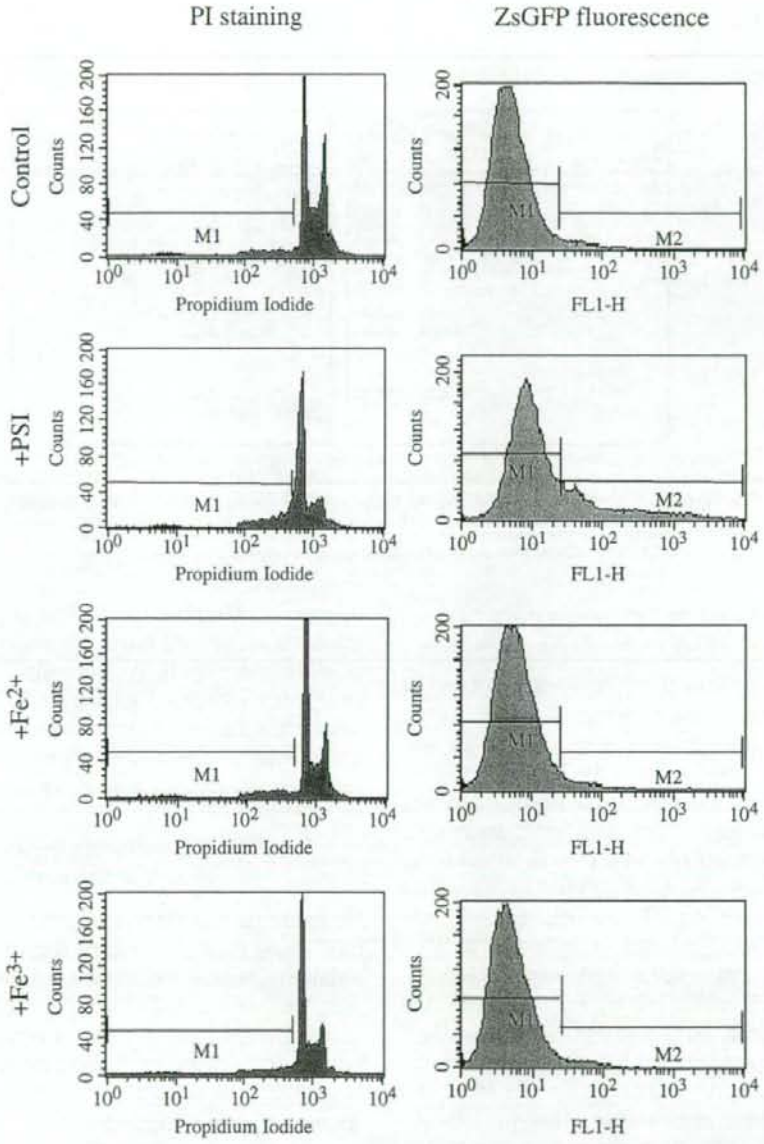

Fig. 6. The cytotoxicity of Fe^{2+} and Fe^{3+} on SH-SY5Y cells transfected with a proteasome sensor vector (SH-PSV cells). SH-PSV cells were cultured in 6-well poly-L-lysine coated flasks with 100 μM of Fe^{2+} or Fe^{3+} for 20 h. The cells were also subjected to FACS and the native fluorescence of ZsGFP, which is coded by proteasome sensor vector, was quantified. At the same time the cells were stained PI solution and subjected to FACS analysis to quantify the apoptotic cells. The number of cells with enhanced ZsGFP were 2.1% in non-treated cells and it increased to 3.1, 3.8 and 20.8%, by 100 μM of Fe^{2+} or Fe^{3+}, or 10 μM of PSI, proteasome inhibitor, respectively. At the same time, apoptotic cells increased from 4.8% in control to 9.6, 7.3 and 23.7% of the total in the presence of Fe^{2+}, Fe^{3+}, and PSI, respectively

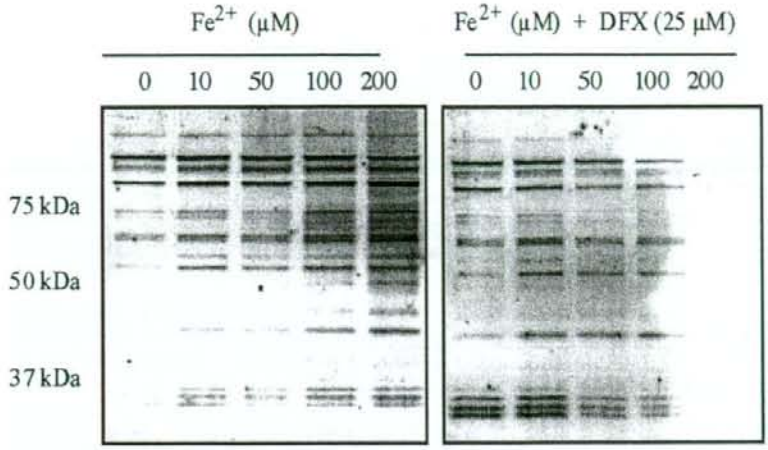

Fig. 7. Fe^{2+} treatment increased acrolein-modified protein in SH-SY5Y cells. SH-SY5Y cells were incubated with various concentrations of Fe^{2+} for 20 h, in the absence and presence of 25 μM deferoxamine mesylate (DFX). Acolein-modified protein was detected by Western blot analysis using antibody against acrolein-protein conjugates

Effect of iron on proteasome activity and viability in SH-SY5Y cells

The effects of iron (Fe^{2+} or Fe^{3+}) on the UP system were studied using SH-PSV cells. As shown in Fig. 4, after cultured in the presence of iron for 20 h, the ZsGFP fluorescence in SH-PSV cells increased in a dose-dependency way. Fe^{2+} and Fe^{3+} increased the accumulation of ZsGFP with almost the same intensity, and DFX (25 μM) suppressed the increase in ZsGFP fluorescence. Ascorbic acid, NAC, reduced glutathione (GSH), (−)-EGCG and α-tocopherol suppressed the accumulation of ZsGFP by Fe^{2+} (Fig. 5). On the other hand, Fe^{2+} and Fe^{3+} did not affect the *in vitro* activity of 20S proteasome samples prepared from SH-SY5Y cells (data not shown). These results show that iron inhibited the UP system, but it is not due to the direct inhibition of 20S proteasome enzymes.

The cytotoxicity of Fe^{2+} and Fe^{3+} was examined by fluorescence-augmented flow cytometry (FACS) after incubated with 100 μM Fe^{2+} and Fe^{3+} for 20 h, and the number of cells with enhanced ZsGFP increased to 3.1 and 3.4% of the total cells from 2.1% in control, whereas 10 μM PSI, a proteasome inhibitor, increased the cell number to 20.8%, as shown in Fig. 6. At the same time, apoptotic cells increased to 9.6 and 7.3% of the total cell number in the presence of Fe^{2+} and Fe^{3+}, and 23.7% in cells treated with PSI, respectively, from 4.8% in control.

Increased acrolein-modified protein by iron treatment

To estimate the effects of iron on lipid peroxidation, acrolein, one of the most reactive aldehyde, was detected with antibody against acrolein-conjugated protein. As shown Fig. 7, acrolein-adducted protein increased in the cells treated with Fe^{2+}, in a dose-dependent way. DFX reduced the amount of acrolein-modified protein significantly.

Discussion

These results clearly demonstrate that NM, in contrast to synthetic dopamine melanin without iron, increases formation of ROS-RNS and induces onset of oxidative stress in mitochondria. In this case, it should be empha-

sized that mitochondria are essentially required for the generation of ROS-RNS. In mitochondria prepared from dopaminergic SH-SY5Y cells, ROS is produced from $O_2^{\bullet -}$ via oxidative phosphorylation, while H_2O_2, at least in part, is generated *via* oxidation of dopamine by monoamine oxidase. About RNS recent reports suggest the existence of nitric oxide synthase in mitochondria (Elfering et al., 2002). In our system using DCF, measurable ROS-RNS species were characterized as $^{\bullet}OH$, $NO^{\bullet}$ and $ONOO^-$, which is produced by a reaction of $NO^{\bullet}$ with $O_2^{\bullet -}$ (Crow, 1997). DFX, an iron chelator, markedly reduced ROS-RNS production, suggesting that iron released form NM catalytically increases these kind of ROS-RNS production in mitochondria. Indeed, iron is well known to increase $^{\bullet}OH$ synthesis from H_2O_2 by the Fenton reaction, or by the Haber-Weiss reaction by the reaction of $O_2^{\bullet -}$ and H_2O_2 (Halliwell, 1992). In the system used in this paper SOD can completely suppresses the increase in DCF by NM, but catalase did not, indicating that the role of H_2O_2 is negligible. On the other hand, we showed that NM increases NO production by mitochondria. These results indicate that NM increased $O_2^{\bullet -}$ and NO simultaneously in mitochondria and produced $ONOO^-$, which is a powerful oxidant that may decompose further to the very reactive $^{\bullet}OH$. It is consistent with our previous data that in SH-SY5Y cells, RNS is the major source of DCF production (Maruyama et al., 2001).

The function of NM has yet to be established, but it is considered as an endogenous iron-binding molecule in pigmented neurons (reviewed in Fedorow et al., 2005b). It may therefore play a physiological role in intraneuronal iron homeostasis. Support for this theory comes from changes in NM in the PD brain where significantly less iron is bound to NM than that seen in the normal brain (Lopiano et al., 1990). This suggests that changes in iron-binding to NM result in increased levels of intraneuronal free iron and the subsequent cell damage observed in PD. Isolated human NM consists of 2.8% iron as estimated by Mössbauer spectroscopy (Gerlach et al., 1995), while the concentration of Fe^{3+} in the SN has been estimated using electron paramagnetic resonance at 6780 ng iron/mg intact SN tissue or 11300 ng iron/mg isolated NM (Shima et al., 1997). Iron binding studies using NM isolated from the human SN demonstrated that NM contains high ($K_d = 7.18 \pm 1.08$ nM) and low-affinity binding sites ($K_d = 94.31 \pm 6.55$ nM) for Fe^{3+} (Double et al., 2003). Our recent data demonstrates that a purely Fe^{3+} signal can be measured from intact frozen SN tissue using Mössbauer spectroscopy (Double et al., 2003). The interaction of iron with NM is of interest because the behaviour of NM changes in the presence of iron; instead of inactivating free radicals, it begins to act as an effective pro-oxidant. Recent *in vitro* studies suggest that iron is releasable under certain circumstances from NM to interact in free radical-producing pathways (Double et al., 1999): In the absence of iron, isolated human NM significantly decreased membranal damage in rat cortical homogenates *in vitro* as measured by lipid peroxidation. Further when NM was added together with iron the amount of lipid peroxidation measured was significantly less than that induced by iron alone. These results support the hypothesis that NM has antioxidant properties and can protect the cell from radical-induced damage. In contrast, when iron-saturated NM was added to the membrane homogenate, cell damage was significantly increased to 264% of that induced by NM alone; this damage was significantly attenuated by the addition of the iron chelator DFX (Double et al., 1999). These data were relevant with the result that iron increased lipid peroxidation product, acrolein-modified proteins. These and the previous results support the hypothesis that NM can have a protective influence on the cell, but can be

detrimental when iron levels rise above a certain level.

Recently we found that mitochondrial dysfunction caused by rotenone, a complex I inhibitor, increased protein modification by acrolein, and reduced the activity of proteasome, through binding of aggregated oxidized protein to the catalytic site of 20S proteasome and direct adduction of acrolein to 20S protosome itself (Shamoto-Nagai et al., 2003). More recently we found that NM inhibited the *in vitro* and *in situ* activity of 26S proteasome in SH-SY5Y cells (Shamoto-Nagai et al., 2004). The results reported here clearly show that NM is a source of cytotoxic iron and induces the onset of oxidative stress in mitochondria leading to the dysfunction. As the result, decreased ATP synthesis and enhanced oxidative stress may induce the deterioration of UP system with increased oxidative-modified proteins, such as acrolein-conjugated ones. The capacity of NM to regulate iron level in the cells may determine the vulnerability of dopamine neurons in aging and PD by initiating the malignant cycle between the mitochondrial dysfunction, increased oxidative stress and impairment of the UP system.

Acknowledgements

This work was supported by a Grant-in-Aid on Scientific Research for Young Scientists (B) for M. S. and (C) (W. M.) and (A) (W. M. and T. O.) from Japan Society for the Promotion of Science, Grant for Research on Dementia and Bone Fracture (W. M., M. N.) from the Ministry of Health, Labor and Welfare, Japan. P.R. was supported by the National Parkinson Foundation, Miami, Florida, USA.

References

Akao Y, Seki N, Nakagawa Y, Yi H, Matsumoto K, Ito Y, Ito K, Funaoka M, Maruyama W, Naoi M, Nozawa Y (2004) A highly bioactive lignophenol derivative from bamboo lignin exhibits a potent activity to suppress apoptosis induced by oxidative stress in human neurobalstoma SH-SY5Y cells. Bioorgan Med Chem 12: 4791–4801

Ben-Shachar D, Riederer P, Youdim MBH (1991) Iron-melanin interaction and lipid peroxidation: implications for Parkinson's disease. J Neurochem 57: 1609–1612

Bradford MM (1976) A rapid and sensitive method for quantitation of microgram quantities of protein using the principle of protein dye binding. Anal Biochem 72: 248–254

Bridelli MG, Tampellini D, Zecca L (1999) The structure of neuromelanin and its iron binding site studied by infrared spectroscopy. FEBS Lett 457: 18–22

Crow JP (1997) Dichlorodihydrofluorescein and dihydrorhodamine 123 are sensitive indicators of peroxynitrite in vivo: implications for intracellular measurement of reactive nitrogen and oxygen species. Nitric Oxide 1: 145–157

D'Amato RJ, Lipman ZP, Snyder SH (1986) Selectivity of the Parkinson neurotoxin, MPTP, toxic metabolite MPP^+ binds to neuromelanin. Science 231: 987–989

Desagher S, Osen-Sand A, Nichols A, Eskes R, Montessuit S, Lauper S, Maundrell K, Antonsson B, Martinou J-C (1999) Bid-induced conformational change of Bax is responsible for mitochondrial cytochrome c release during apoptosis. J Cell Biol 144: 891–901

Double KL, Riederer P, Gerlach M (1999) The significance of neuromelanin for neurodegeneration in Parkinson's disease. Drug News Perspect 12: 333–340

Double KL, Zecca L, Costi P, Mauer M, Griesinger C, Ito S, Ben-Shachar D, Bringmann G, Fariello RG, Riederer P, Gerlach M (2000) Structural characteristics of human substantia nigra neuromelanin and synthetic dopamine melanins. J Neurochem 75: 2583–2589

Double KL, Ben-Shachar D, Youdim MBH, Zecca L, Riederer P, Gerlach M (2002) Influence of neuromelanin on oxidative pathways within the human substantia nigra. Neurotoxicol Teratol 24: 621–628

Double KL, Gerlach M, Schünemann V, Trautwein AX, Zecca L, Gallorini M, Youdim MBH, Riederer P, Ben-Shachar D (2003) Iron binding characteristics of neuromelanin of the human substantia nigra. Biochem Pharmacol 66: 489–494

Dzierzega-Lecznar A, Kurkiewicz S, Chodurek E, Stepien K, Wilczok T, Arzberger A, Riederer P, Gerlach M (2004) Neuromelanin of the human substantia nigra: structural investigations by pyrolysis-gas chromatography/mass spectrometry. J Am Soc Mass Spectrometry 15: 920–926

Eckert A, Steiner B, Marques C, Leutz S, Roming H, Haass C, Muller WE (2001) Elevated vulnerability to oxidative stress-induced cell death and activation